



Large-scale structures and spatial clustering of X-ray sources in the Chandra Msec Fields

R. Gilli

INAF - Osservatorio Astrofisico di Arcetri, Largo E. Fermi 5, 50125 Firenze, Italy e-mail: gilli@arcetri.astro.it

Abstract. The redshift distribution of the X-ray sources (mainly AGN) identified so far in the 1Msec *Chandra* Deep Field South (CDFS) is characterized by several spikes. The most prominent features, at $z = 0.67$ and $z = 0.73$, contain about 1/3 of the identified sources. Similar redshift spikes, although less prominent, have been also observed in the 2 Msec *Chandra* Deep Field North (CDFN). The clustering properties of the CDFS and CDFN sources have been measured via the projected correlation function $w(r_p)$. The AGN clustering amplitude is found to be a factor of ~ 2 higher in the CDFS than in the CDFN, revealing large cosmic variance in these 0.1 deg^2 fields. The extra correlation signal in the CDFS is due to the two identified structures at $z = 0.67$ and $z = 0.73$. Within each field, no significant differences are found between the clustering properties of soft and hard X-ray selected sources, or, similarly, between those of type 1 and type 2 AGN. The high ($5 - 10 h^{-1} \text{ Mpc}$) correlation length measured for AGN at $z \sim 1$ in the two *Chandra* Msec fields is comparable to that of early type galaxies at the same redshift.

Key words. Surveys – Galaxies: active – X-rays: general – Cosmology: large-scale structure of Universe

1. Introduction

Active Galactic Nuclei (AGN) are one of the best tools to study the large scale structure of the Universe at intermediate-high redshifts, $z \sim 1 - 2$, i.e. at an epoch where matter was undergoing the transition from the initially smooth state observed at the recombination to the clumpy distribution observed at present time (Hartwick & Schade 1990). The AGN spatial clustering has been directly measured by means of optical surveys encompassing an increasing number of QSO (Shanks et al. 1987; Grazian et al. 2004; Croom et al. 2001), but in the X-ray band, where the bulk of the obscured AGN population should emerge

(e.g. Comastri et al. 1995; Gilli et al. 2001; Ueda et al. 2003), this is still poorly constrained. Significant clustering signal in the X-rays has been detected from angular correlations (Vikhlinin & Forman 1995; Giacconi et al. 2001; Akylas et al. 2000; Yang et al. 2003; Basilakos et al. 2004), which have been often converted into spatial correlations by assuming an *a priori* redshift distribution. Unfortunately, because of the several uncertainties in its assumptions, this method has not provided stringent results. To date, the only direct measurement of the spatial correlation function of X-ray selected AGN, usually approximated by a powerlaw $\xi(r) = (r/r_0)^{-\gamma}$, has been obtained by Mullis (2001), who found $r_0 = 6.8 \pm 1.6 h^{-1}$

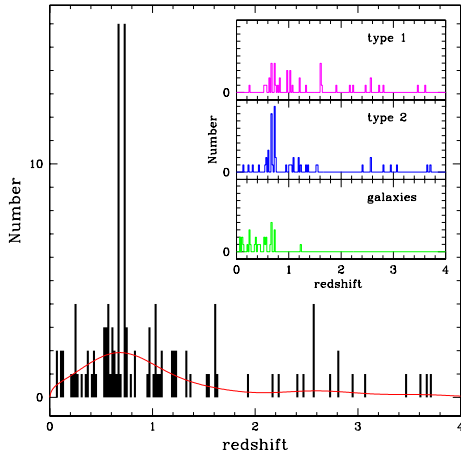


Fig. 1. Redshift distribution for CDFS sources in bins of $\Delta z = 0.02$. The solid curve shows the smoothed distribution used to calculate $w(r_p)$ (see text). The inset shows the redshift distribution for different source classes.

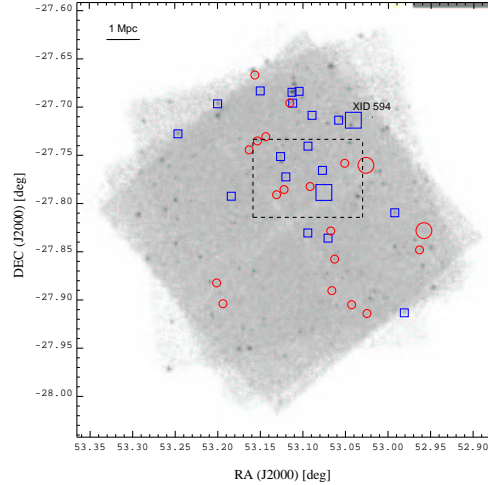


Fig. 2. *Chandra* ACIS-I image of the CDFS with X-ray sources at $z = 0.67$ and $z = 0.73$ marked with circles and squares, respectively. Extended sources are represented as large symbols. The dashed box indicates the region covered by the K20 survey (Cimatti et al. 2002).

Mpc for the AGN in the ROSAT NEP survey (the slope was fixed to $\gamma = 1.8$). Because of the short exposure times and the ROSAT limited sensitivity only bright sources, with a surface density of $\sim 3 \text{ deg}^{-2}$, were detected in the NEP survey. Since the spatial correlation function is a power law increasing at lower pair separations, deep pencil beam surveys like the 1Msec *Chandra* Deep Field South (CDFS; Rosati et al. 2002; Giacconi et al. 2002) and the 2Msec *Chandra* Deep Field North (CDFN; Alexander et al. 2003; Barger et al. 2003), where the X-ray source surface density is about $3000\text{--}4000 \text{ deg}^{-2}$, are expected to provide the highest signal significance with the minimum number of identified objects. The drawbacks are that these strong signals may be subject to substantial variance on small areas, so that the “real” amplitude of the correlation would need a large set of measurements in independent fields to be reliably estimated.

2. Large scale structures in the CDFS

In the 1Msec ACIS-I observation of the CDFS a total of 346 X-ray sources have been de-

tected over the whole 0.1 deg^2 field (Rosati et al. 2002; Giacconi et al. 2002). In the center of the field limiting fluxes of $5.5 \cdot 10^{-17} \text{ erg cm}^{-2} \text{ s}^{-1}$ and $4.5 \cdot 10^{-16} \text{ erg cm}^{-2} \text{ s}^{-1}$ have been achieved in the 0.5-2 keV (soft) and 2-10 keV (hard) band, respectively. So far 127 high quality redshifts with two or more identified lines ($\sim 35\%$ of the total sample) have been obtained by means of VLT spectroscopy (Szokoly et al. 2004). The spectroscopic completeness increases to 78% when considering X-ray sources with optical counterparts brighter than $R = 24$. As shown in Fig. 1 the redshift distribution is dominated by two large concentrations of sources at $z = 0.67$ and $z = 0.73$, while other smaller peaks are also visible (e.g. Gilli et al. 2003). The distribution on the sky of the sources in the two spikes is shown in Fig. 2. A few of them are extended in the X-rays (one is shown in Fig. 3), corresponding to galaxy groups/clusters embedded in larger structures, thus providing a beautiful sketch of the cosmic web. About 1/10 of the X-ray field has been covered by the K20 near-infrared survey (Cimatti et al. 2002). Similarly to the X-

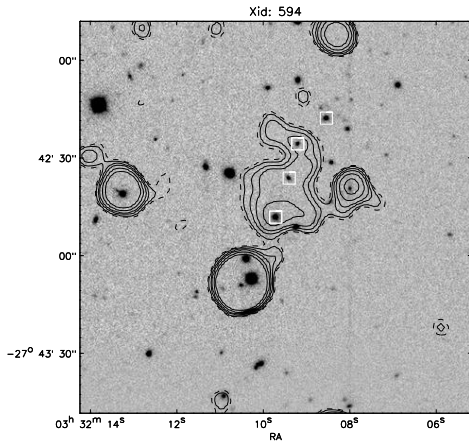


Fig. 3. R band image (60×60 arcsec) of the extended X-ray source XID 594 in the CDFS with X-ray contours overlaid (Szokoly et al. 2004). Four identified objects at $z = 0.73$ are marked with squares.

ray data, the redshift distribution of the galaxies identified in the K20 survey has two prominent peaks at $z = 0.67$ and $z = 0.73$. Moreover, at $z < 1.3$, where the K20 survey is more sensitive, there is almost a one-to-one correspondence between less prominent X-ray and K20 redshift spikes (Gilli et al. 2003).

3. The spatial correlation function in the CDFS and CDFN

Gilli et al. (2004) measured quantitatively the clustering level of CDFS sources by means of the projected correlation function $w(r_p)$ (Davis & Peebles 1983). For comparison $w(r_p)$ was also calculated for the ~ 250 X-ray sources with robust spectroscopic redshift identified so far in the CDFN (Barger et al. 2003). The redshift distribution for the considered CDFN sample is shown in Fig. 4. As in the case of the CDFS redshift distribution, several spikes, although less prominent than those of the CDFS, can be immediately recognized (Barger et al. 2003). To measure the clustering properties of different source populations, the X-ray hardness ratio vs. X-ray luminosity diagram pre-

sented by Szokoly et al. (2004) was used to classify the X-rays sources as type-1 AGN, type-2 AGN and galaxies.¹

To avoid distortions due to peculiar velocities, the spatial clustering of CDFS and CDFN sources was estimated by means of the projected correlation function $w(r_p)$ (Davis & Peebles 1983) which can be easily related to the real-space correlation function $\xi(r)$, which essentially measures the excess of source pairs at a given separation with respect to a random distribution. The minimum variance estimator proposed by Landy & Szalay (1993) to measure $\xi(r)$ was used, and special care was taken in creating the random control sample. In particular the objects in the random sample were placed at the coordinates of the real sources, and their redshifts were extracted from a smoothed distribution of the observed one (see Fig. 1 and Fig. 4). This procedure was extensively tested and found to be appropriate for the CDFS and CDFN samples (Gilli et al. 2004). The projected correlation function $w(r_p)$ was measured at different scales r_p and the best fit parameters γ and r_0 were determined via χ^2 minimization. We note that while

¹ That scheme was somewhat simplified by avoiding the luminosity distinction between type-2 AGN/QSOs and between type-1 AGN/QSOs.

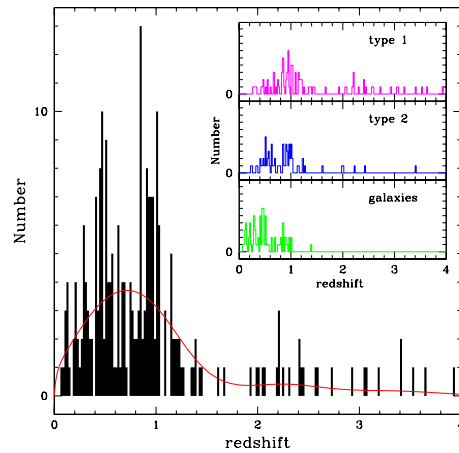


Fig. 4. Same as in Fig. 1 but for CDFN sources.

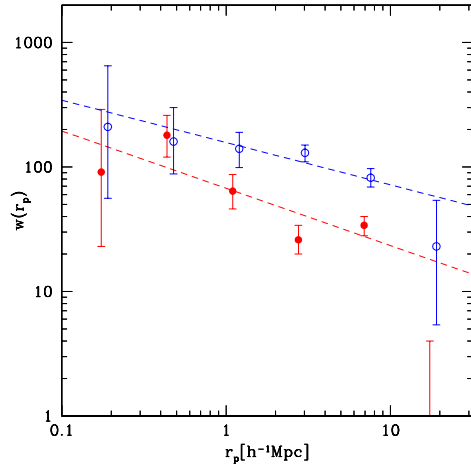


Fig. 5. AGN projected correlation functions in the CDFN (filled circles) and CDFS (open circles). Errors are 1σ Poisson confidence intervals. The best fit power laws are shown as dashed lines.

Poisson errorbars underestimate the true uncertainties on the r_0 and γ values when the source pairs are not independent, bootstrap resampling techniques (Mo, Jing, & Börner 1992), which are often used to circumvent this problem, may substantially overestimate the real uncertainties. In the considered samples bootstrap errors are a factor of ~ 2 larger than Poissonian errors (Gilli et al. 2004). In the following we will then simply quote r_0 and γ together with their 1σ Poisson errors, bearing in mind that the most likely uncertainty lays between the quoted number and its double. A flat cosmology with $\Omega_m = 0.3$ and $\Omega_\Lambda = 0.7$ is assumed; comoving distances in units of h^{-1} Mpc are quoted, where $H_0 = 100 h \text{ km s}^{-1}$.

3.1. Results

Both in the CDFS and CDFN the clustering level of the total X-ray samples is dominated by that of AGN, which indeed represent the majority of the identified sources. In both fields the correlation function is measured on scales $r_p = 0.16 - 20 h^{-1}$ Mpc for AGN at a median redshift of $z \sim 0.9$ and with median X-

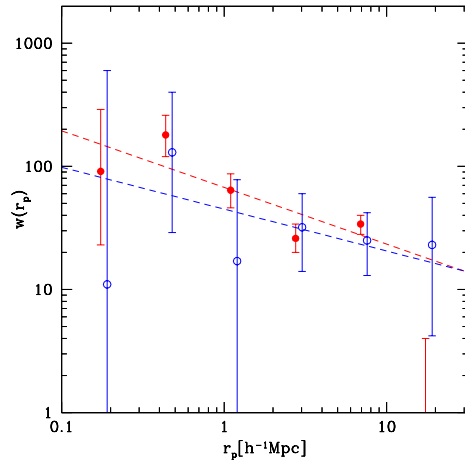


Fig. 6. Projected correlation function for the total CDFN sample (filled circles) and the CDFS sample obtained by excluding sources in the two spikes at $z=0.67$ and $z=0.73$ (open circles). Errors are 1σ Poisson confidence intervals. The best fit power laws are shown as dashed lines.

ray luminosity of $L_{0.5-10} \sim 10^{43} \text{ erg s}^{-1}$, i.e. in the Seyfert luminosity regime. The best fit parameters of the AGN correlation function were found to be $r_0 = 10.3 \pm 1.7 h^{-1}$ Mpc, $\gamma = 1.33 \pm 0.14$ in the CDFS and $r_0 = 5.5 \pm 0.6 h^{-1}$ Mpc, $\gamma = 1.50 \pm 0.12$ in the CDFN (see Fig. 5). As verified by Gilli et al. (2004), the difference in the r_0 values between the two fields is not due to observational biases affecting in different ways the two samples (i.e. different X-ray sensitivity or spectroscopic incompleteness), but is rather due to genuine cosmic variance. Indeed, while in the CDFS about 1/3 of the identified sources lay within the two spikes at $z = 0.67$ and $z = 0.73$, no such prominent features are observed in the CDFN (for comparison the two most populated spikes of the CDFN contain only 1/8 of the identified sources). As shown in Fig. 6, when excluding the sources in the two spikes at $z = 0.67$ and $z = 0.73$, the correlation length measured for CDFS AGN is found to be in good agreement with that measured for CDFN AGN.

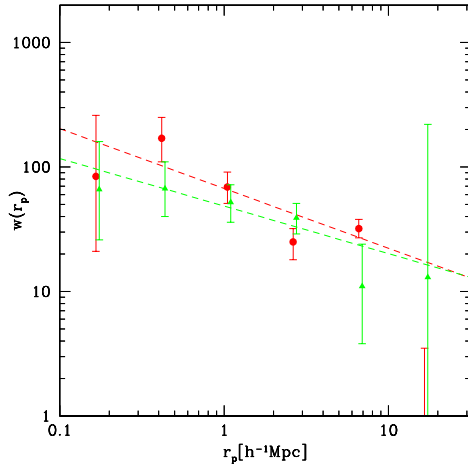


Fig. 8. Projected correlation functions for AGN (circles) and galaxies (triangles) in the CDFN. Errors are 1σ Poisson confidence intervals. The best fit power laws are shown as dashed lines.

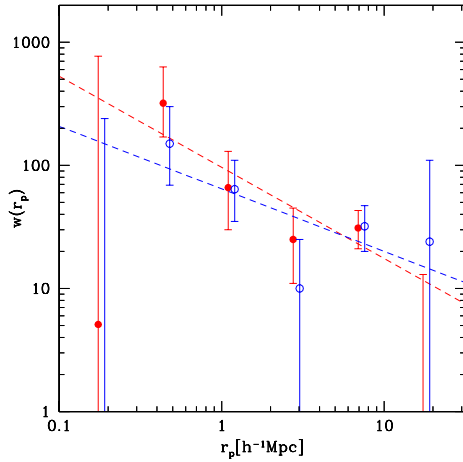


Fig. 7. Projected correlation functions for type 1 AGN (filled circles) and type 2 AGN (open circles) in the CDFN. Errors are 1σ Poisson confidence intervals. The best fit power laws are shown as dashed lines.

The slope of the correlation, $\gamma = 1.3 - 1.5$, is flatter than that commonly observed for galaxies ($\gamma \sim 1.6 - 2.0$, Le Fevre et al. 1996;

Guzzo et al. 1997) but is consistent within the errors with the value of $\gamma = 1.56 \pm 0.10$ measured for the sample of $> 10^4$ optically selected QSO in the 2QZ survey (Croom et al. 2001). We note that, when fixing the slope of the correlation to $\gamma = 1.8$, the best fit r_0 values measured in the CDFS and in the CDFN increase by only 15%. Within each field no significant clustering differences are found between soft and hard X-ray selected sources, or, similarly, between type-1 and type-2 AGN. The comparison between the clustering properties of type-1 and type-2 AGN in the CDFN is shown in Fig. 7: although the two correlations seem to have different slopes and amplitudes, they are in agreement within the errors. In the CDFN, where the source statistics is sufficiently high, the clustering of X-ray selected galaxies was also measured and compared with that of AGN (see Fig. 8). Again, due to the relatively large errors, no significant differences can be claimed.

4. Final remarks

The good correspondence between the redshift peaks of X-ray and K-band selected sources in the CDFS (Gilli et al. 2003) supports the idea that Seyfert-like AGN clustering is similar to that of early type galaxies, whose detection rate is higher in K-band rather than in optically selected samples. In the CDFS this is directly confirmed, since the measured r_0 value for AGN is similar to that of Extremely Red Objects (i.e. galaxies with $R - K > 5$) at the same redshift ($z \sim 1$), which are thought to be the progenitors of early type galaxies (Daddi et al. 2001). When considering the lower amplitude observed in the CDFN, we can estimate the correlation length of the AGN in the *Chandra* Msec fields to be in the range $5 - 10 h^{-1}$ Mpc, which this is still consistent with Seyfert-like AGN at $z \sim 1$ to be generally hosted by early type galaxies (Coil et al. 2003 found $r_0 = 5.5 - 7.7 h^{-1}$ Mpc and $r_0 = 2.6 - 3.7 h^{-1}$ Mpc for early and late type galaxies at $z \sim 1$, respectively).

Acknowledgements. All this work has been done in collaboration with many people in the CDFS and

K20 team who I gratefully acknowledge: E. Daddi, G. Zamorani, P. Tozzi, S. Borgani, J. Bergeron, R. Giacconi, G. Hasinger, V. Mainieri, C. Norman, P. Rosati, G. Szokoly, W. Zheng, A. Cimatti, L. Kewley, M. Nonino, J.X. Wang, M. Mignoli, A. Zirm.

References

- Alexander, D.M., Bauer, F.E., Brandt, W.N., et al. 2003, *AJ* 126, 539
- Akylas, A., Georgantopoulos, I., Plionis, M. 2000, *MNRAS* 318, 1036
- Barger, A.J., Cowie, L.L., Capak, P., et al. 2003, *AJ* 126, 632
- Basilakos S., et al. 2004, *ApJL* in press (astro-ph/0404413)
- Cimatti, A., Mignoli, M., Daddi, E., et al. 2002, *A&A* 392, 395
- Coil, A.L., et al. 2003, *ApJ* in press (astro-ph/0305586)
- Comastri, A., Setti, G., Zamorani, G., Hasinger, G. 1995, *A&A* 296, 1
- Croom, S.M., Shanks, T., Boyle, B.J., Smith, R.J., Miller, L., Loaring, N.S., Hoyle, F. 2001, *MNRAS* 325, 483
- Daddi, E., et al. 2001, *A&A* 376, 825
- Davis, M., & Peebles, P.J.E. 1983, *ApJ* 267, 465
- Giacconi, R., Rosati, P., Tozzi, P., Nonino, M., Hasinger, G., Norman, C., Bergeron, J., Borgani, S., Gilli, R., Gilmozzi, R. & Zheng, W. 2001, *ApJ* 551, 624
- Giacconi, R., Zirm, A., Wang, et al. 2002, *ApJS* 139, 369
- Gilli, R., Salvati, M., & Hasinger, G. 2001, *A&A* 366, 407
- Gilli, R., Cimatti, A, Daddi, E., et al. 2003, *ApJ* 592, 721
- Gilli, R., et al. 2004, *A&A* submitted
- Grazian, A., Negrello, M., Moscardini, L., et al. 2004, *ApJ* in press (astro-ph/0303382)
- Guzzo, L., Strauss, M.A., Fisher, K.B., Giovanelli, R., Haynes, M.P. 1997, *ApJ* 489, 37
- Hartwick, F.D.A. & Schade, D. 1990, *ARA&A* 28, 437
- Landy, S.D., & Szalay, A.S. 1993, *ApJ* 412, 64
- Le Fevre, O., Hudon, D., Lilly, S. J., Crampton, David, Hammer, F., Tresse, L. 1996, *ApJ* 461, 534
- Mo, H.J., Jing, Y.P., & Börner, G. 1992, *ApJ* 392, 452
- Mullis, C.R. 2001, Ph.D. thesis,
- Rosati, P., Tozzi, P., Giacconi, R., et al. 2002, *ApJ* 566, 667
- Shanks, T., Fong, R., Boyle, B.J., Peterson, B.A. 1987, *MNRAS* 277, 739
- Szokoly, G., Bergeron, J., Hasinger, G., et al. 2003, *ApJS* submitted, astro-ph/0312324
- Ueda, Y., Akiyama, M., Ohta, K., Miyaji, T. 2003, *ApJ*, 598, 886
- Vikhlinin, A., Forman, W. 1995, *ApJ*, 455, L109
- Yang, Y., Mushotzky, R. F., Barger, A. J., Cowie, L. L., Sanders, D. B., Steffen, A. T. 2003, *ApJ* 585, L85